


Sertraline Alleviates Chronic Prostatitis by Regulating the TRPV1 Channel

Yongfeng Lao ^{1,2}, Yanan Bai^{1,2}, Xin Guan^{1,2}, Jian Wang^{1,2}, Yanan Wang^{1,2}, Rongxin Li^{1,2}, Yongqiang Ding^{1,2}, Zhilong Dong^{1,2}

¹Second Clinical Medical College, Lanzhou University, Lanzhou, Gansu, People's Republic of China; ²Department of Urology, The Second Hospital of Lanzhou University, Lanzhou, Gansu, People's Republic of China

Correspondence: Zhilong Dong, Department of Urology, The Second Hospital of Lanzhou University, No. 82, Cuiyingmen, Chengguan District, Lanzhou, Gansu, People's Republic of China, Email dzl1997.student@sina.com

Introduction: Although sertraline has been widely used for chronic prostatitis (CP), the mechanisms are unclear. Herein, we explored the mechanisms of sertraline in treating CP.

Methods: Network pharmacology methods were used to explore the potential targets and molecular mechanisms. LPS was used to stimulate RWPE-1 cells to construct an in vitro model of CP. An experimental autoimmune prostatitis (EAP) mice model was built. CCK-8 assay, EdU assay, BrdU detection, and Tunel assay were performed to evaluate the proliferation and apoptosis process of cells or tissues, respectively. DCFH-DA and Fluo-4 fluorescence probes were used to detect intracellular ROS and calcium concentrations. Von Frey filaments and open-field tests were utilized to evaluate pain response and depressive-like behavior of mice. Histopathology was evaluated through hematoxylin and eosin staining. RT-qPCR, Western blot, immunofluorescence, and immunohistochemistry were utilized to evaluate the transcription, expression, and location of related proteins. Molecular dynamics (MD) simulation and surface plasmon resonance (SPR) assay were performed to measure the binding capacity of sertraline and related proteins.

Results: Through a network pharmacology analysis, 27 potential targets of sertraline for CP were obtained, and 5 key targets (CHRM1, ADRA1B, HTR2B, HTR2A, and TRPV1) were finally identified. Functional experiments suggested that TRPV1 was involved in the proliferation, apoptosis inhibition, and ROS production of LPS-induced RWPE-1 cells. In vitro experiments showed that sertraline significantly inhibited cell proliferation, ROS generation, and transcription of inflammation cytokines of LPS-induced RWPE-1 cells. Additionally, sertraline markedly promoted the apoptosis level of LPS-stimulated RWPE-1 cells and elevated the expression level of BAX while reducing the expression levels of Bcl2 and Caspase-3. MD simulation and SPR assay confirmed the direct binding of sertraline to TRPV1. Moreover, sertraline significantly down-regulated the expression level of TRPV1 and inhibited calcium influx of LPS-induced RWPE-1 cells. TRPV1 agonist (Capsaicin) significantly restored the effects on proliferation, apoptosis, ROS production, and calcium influx of sertraline on LPS-induced RWPE-1 cells. Mice experiments demonstrated that sertraline treatment could reduce pain response, improve depression-like symptoms, and relieve local prostate inflammation of EAP mice, as well as down-regulated the expression level of TRPV1, inhibit the proliferation, and promote apoptosis of prostate tissues in EAP mice.

Discussion: The results revealed the anti-inflammatory effect of sertraline for RWPE-1 cells and EAP mice, and the potential mechanism was regulating the TRPV1 channel. It indicated that sertraline might serve as a complementary anti-inflammatory agent for CP.

Keywords: chronic prostatitis, sertraline, RWPE-1, mice, TRPV1

Introduction

Chronic prostatitis (CP) is one of the most common urologic diseases, while 35%-50% of men reported being affected by symptoms suggesting prostatitis during their lifetime.¹ A systematic review based on a population of >10,000 participants found an 8.2% prevalence of prostatitis-related symptoms.² The etiological mechanism of CP is complex and has not yet been fully clarified, which may be related to infection, urine regurgitation, psychopsychological factors, neuroendocrine

factors, pelvic floor muscle dysfunction, and immune dysfunction.^{1,3} To date, there is still a lack of effective strategies for the management of CP.^{4,5}

A prospective cohort found that patients with CP had a significantly increased risk of depression over the next 3 years.⁶ Another retrospective cohort study found an elevated risk of CP in patients with depression.⁷ Barone et al found that subjects who suffered anxiety and stress showed worse prostatitis-related symptoms, suggesting a significant role of mental health in symptoms perception of CP.⁸ Due to high comorbidity rates of psychological symptoms and sexual dysfunction, traditional or new selective serotonin reuptake inhibitors (SSRIs) such as sertraline (SERT) and dapoxetine have been widely used in CP associated with concomitant symptoms. Our previous network meta-analysis systematically evaluated the efficacy and safety of SSRIs in CP.⁹ The results demonstrated the extra benefit of SSRIs in patients with CP, while SERT might behave optimally in CP, especially when combined with depressive symptoms. As one of the most popular antidepressants, SERT works by inhibiting synaptosomal 5-HT uptake *in vitro* and *in vivo* and slightly inhibiting noradrenaline and dopamine uptake.¹⁰ However, the effect mechanism of SERT for CP is still unclear, which limits the indication of SERT in the treatment of CP. Whether the SSRIs improve the concomitant symptoms to relieve prostatitis-related symptoms or just directly improve prostatic inflammation needs to be urgently clarified, influencing the clinical indications of SSRIs for CP.

Therefore, network pharmacology strategy, *in vitro* and *in vivo* experiments were utilized to explore the potential effect mechanism of SERT for CP in this study. Our results might provide a theoretical basis for the detailed mechanism exploration of SSRIs for CP in the future.

Materials and Methods

SSRIs and CP-Related Targets Screening

The chemical structure of the SERT was first obtained from the PubChem database.¹¹ The structure was then uploaded to the SwissTargetPrediction database under “Homo Sapiens” mode to retrieve the targets of SERT.¹² CP-related targets were screened via GeneCards,¹³ DisGeNET,¹⁴ and OMIM¹⁵ databases. The results of each dataset were summarized. “Chronic prostatitis” was used as the key term for target retrieval. The overlapped targets of SERT and CP were obtained using the Venn diagram.

Construction of the PPI Network

The STRING database was used for protein–protein interaction (PPI) network construction.¹⁶ Cytoscape software 3.9.0 was utilized to determine the genes’ degree and better visualize the PPI network. The Cytoscape plugin “cytoHubba” was adopted to identify the top 10 targets with the highest degrees in the PPI network.

Go Enrichment and KEGG Pathway Analysis

The DAVID database was used for the function enrichment analysis of the overlapped targets of SERT and CP.¹⁷ The gene background was chosen as “homo sapiens”. The results of Gene Ontology (GO) and Kyoto Encyclopedia of Genes and Genomes (KEGG) pathway analysis were visualized utilizing R software 4.1.2. All the results of KEGG were exhibited, while only the top 10 of GO terms were presented.

Construction of the “Drug-Target-Pathway” Network

The KEGG results of SERT associated with enriched genes were imported to Cytoscape software 3.9.0 for the construction of a “target-pathway” network.

Molecular Docking

The two-dimensional (2D) structure of the drug ligands was downloaded from the PubChem database.¹¹ The three-dimensional (3D) structure of the protein targets was obtained from the Protein Data Bank (PDB) database.¹⁸ If there was no structural information on one protein in the PDB database, the predicted structure would be adopted from the AlphaFold Protein Structure Database.^{19,20} AutoDock Tools 1.5.6 was utilized for the molecular docking of ligands and

protein receptors. The results of docking were visualized in PyMOL software 2.5.4. The threshold representing the active ligand on target was <-6.0 kcal/mol.^{15,21}

Molecular Dynamics Simulation

GROMACS (version 2022.3) was used to conduct molecular dynamics (MD) simulation of SERT with TRPV1^{22,23} to test the structural stability of the protein-ligand complex. In the MD simulation, the Amber99sb-ildn force field and the TIP3P water model were utilized, and the system was neutralized with the required Na⁺. MD simulation was performed at 298.15k and 1 Bar for 100ns. RMSD, RMSF, and radius of gyration (Rg) were calculated to evaluate the structural stability of the protein-ligand complex. The MMPBSA method was used to calculate the binding free energy.²⁴

Material and Reagents

SERT was obtained from Solarbio (SS9970; Beijing, China). Capsazepine (TRPV1 antagonist, HY-15640) and Capsaicin (TRPV1 agonist, HY-10448) were obtained from MedChemExpress (New Jersey, USA). LPS was obtained from Beyotime (S1732; Shanghai, China). Complete Freund's adjuvant (CFA) was purchased from Sigma-Aldrich (F5881; USA). Fluo-4 Calcium Assay Kit was obtained from Beyotime (S1061S; Shanghai, China). CCK-8 assay kit was bought from Sunview (CK001-01; Shenzhen, China). EdU cell proliferation kit was purchased from Beyotime (C0071S; Shanghai, China). Tunel assay kit was obtained from Beyotime (C1088: green fluorescence, C1090: red fluorescence; Shanghai, China). The ROS detection kit was purchased from Abbkine (KTB1910; Wuhan, China). DAPI was purchased from Beyotime (C1006; Shanghai, China). RIPA lysis buffer was also purchased from Beyotime (P0013B; Shanghai, China). The protein loading buffer was obtained from Solarbio (P1041; Shanghai, China). The rapid blocking buffer was purchased from Yoche (YWB0100; Shanghai, China). Primary antibodies against Bcl2 (T40056) and Caspase-3 (T40044) were obtained from Abmart (Shanghai, China). Primary antibody against BAX was purchased from ABclonal (A19684; Wuhan, China). Primary antibodies against β -actin (66,009-1-Ig), GAPDH (60004-1-Ig), and TRPV1 (66,983-1-Ig) were purchased from Proteintech (Wuhan, China). Primary antibody against BrdU was obtained from Abcam (ab152095; Cambridge, UK). Fluorescent secondary antibody for rabbit antibodies was purchased from LI-COR Biotechnology (D11103-05; Nebraska, USA). The fluorescent secondary antibody for mouse antibodies was purchased from Abbkine (A23710; Wuhan, China). Paraformaldehyde was purchased from Biosharp (BL539A; Hefei, China). Normal goat serum for immunofluorescence was obtained from Abbkine (BMS0050; Wuhan, China). CoraLite488-conjugated goat anti-mouse IgG (H+L)(SA00013-1), CoraLite594-conjugated goat anti-mouse IgG (H+L)(SA00013-3), and CoraLite488-conjugated goat anti-rabbit IgG (H+L)(SA00013-2) for immunofluorescence were purchased from Proteintech (Wuhan, China).

Cell Culture and Stimulation

Human prostatic epithelial cell line RWPE-1 (obtained from the cell bank of the Chinese Academy of Sciences, catalog number: SCSP-5025) was cultured in DMEM medium supplemented with 10% fetal bovine serum (FBS). The cells were cultured in a humidified 37°C incubator with 5% CO₂. To generate the in vitro model of chronic nonbacterial prostatitis (CNP), 10 μ g/mL LPS was used to stimulate the cells.

Experimental Autoimmune Prostatitis (EAP) Mice Model and Intervention

All animal experiment procedures were approved by the Experimental Animal Welfare Ethics Committee of the Second Hospital of Lanzhou University (approval number: D2024-430). A total of 18 male C57BL/6J mice were bought from the Laboratory Animal Center of Lanzhou University, and were kept at Lanzhou University's SPF laboratory animal facility. All mice were randomly divided into three groups (Control, EAP, and EAP+SERT). The EAP mouse model was built by referring to the previous method.²⁵⁻²⁷ Briefly, mice in the EAP and EAP+SERT groups were immunized with an emulsion containing equal volumes of CFA and Sprague-Dawley rat male accessory gland (MAG) extract. The emulsion was injected subcutaneously into three sites: the shoulder (50 μ L), the bilateral foot pads (25 μ L each side), and the base of the tail (50 μ L). The EAP mouse model was established by two antigen immunizations on Days 0 and 28. Mice in the Control group were injected subcutaneously with the same amount of saline during immunization. After the model was

built, mice in EAP+SERT were intraperitoneally injected with SERT 10mg/kg/day for two weeks. The experiment concluded on Day 42, and all the mice were humanely euthanized.

Proliferation Detection

Cell proliferation was evaluated by CCK-8 assay. Approximately 1×10^4 RWPE-1 cells were seeded in the 96-well plates each well and cultured to adherent. To evaluate the cytotoxic effect of a drug, different concentrations of drugs were added to the RWPE-1 cells for 12h. To explore the antiproliferative effects of the drug, RWPE-1 cells were pre-treated with the drug for 12h, and then the cells were incubated with LPS for 24h. After drug stimulation, 10 μ L CCK-8 solution was added to each well, and incubated at 37°C for 1h. Finally, the absorbance measurements at 450 nm were read. Additionally, cell proliferation status under different treatments was also assessed by EdU assay according to the instructions provided in the manual of the EdU cell proliferation kit. Proliferation of prostate tissues was evaluated by 5-bromo-2'-deoxyuridine (BrdU) in vivo labeling and subsequent fluorescence detection. The day before humane euthanasia, the mice were intraperitoneally injected 2mg BrdU. After collecting the tissue, the tissue sections were prepared for immunofluorescence detection of BrdU.

Apoptosis Analysis

The cell apoptosis process under the impact of drug treatment was measured using a TUNEL assay kit according to the manufacturer's instructions. Briefly, a total of 2×10^4 cells/well were grown into 24-well plates. After cell adherence and drug treatment, the RWPE-1 cells were fixed with 4% paraformaldehyde for 30 min at room temperature, and then the cells were permeated by 0.3% Triton X-100 for 5 min. Finally, the cells were incubated with TUNEL solution for 1h in the dark at 37°C. The change in apoptosis was captured under a fluorescence microscope. TUNEL-positive cells were apoptotic cells. Apoptosis level of prostate tissues was also evaluated utilizing a TUNEL assay kit. After collecting the tissue, the tissue sections were prepared. After the sections were fixed and permeated, the TUNEL detection solution was added to the sections for incubation for 1h in the dark at 37°C. Finally, fluorescent detection is performed.

ROS Assay

The ROS level in RWPE-1 cells was detected utilizing the DCFH-DA fluorescence probe. Briefly, RWPE-1 cells were seeded to 6-well plates with 1×10^5 cells per well. After drug stimulation, the cells were incubated with 10 μ M DCFH-DA dissolved in a 2mL serum-free medium away from light for 30 min at 37°C. The DCFH-DA probe was then removed and the cells were washed with serum-free medium twice. Finally, the fluorescent signal was captured using a fluorescence microscope to calculate the mean fluorescence intensity of RWPE-1 cells under different treatments.

Detection of the Intracellular Calcium Level

The calcium-sensitive fluorescent indicator Fluo-4 was used to detect the intracellular calcium level and visualize the calcium signal. Firstly, for the quantitative analysis of intracellular calcium level, RWPE-1 cells were seeded to 96-well plates with 2×10^4 cells per well. After drug treatment, the cells were incubated with 100 μ L Fluo-4 staining solution at room temperature for 30 min according to the instruction book. Then, the fluorescent signal of calcium in RWPE-1 cells was detected at a fluorescent microplate reader (Ex/Em=490/525 nm). Furthermore, the calcium signal was also imaged and was also captured under the fluorescence microscope. Briefly, RWPE-1 cells were seeded to 24-well plates with 2×10^4 cells per well. After drug treatment, the cells were incubated with 250 μ L Fluo-4 staining solution. The other details are consistent with the above protocol.

Animal Behavior Testing

Von Frey filaments were used to evaluate for allodynia in the lower abdominal area near the prostate as previously described.^{26,28} Before testing, the mice were allowed to acclimate to the new environment for 30 min. Then, different forces of von Frey filaments: 0.04, 0.16, 0.4, 1.0, 2.0 and 4.0g were utilized to determine the tactile allodynia and hyperalgesia in the lower abdominal of the mice. Each force was tested 50 times. Each test involved 1–2s of filament application, followed by a 5-s interval before the next test. Stimulated points were randomly selected inside the designated area. Any of the following was considered a positive filament stimulation reaction: (1) sudden abdominal flinching, (2) instantaneous licking or scraping of the stimulated area, and (3) leaping. The depressive-like behaviors of

mice were measured by open-field tests.²⁹ The apparatus consisted of an open-field arena (40 × 40 × 40cm). Each mouse was placed separately in the field and was allowed to freely explore for 5 min. The field was cleaned between each test. The test process of each mouse was recorded as a video, and the behavior trajectory was analyzed by ImageJ AnimalTracker Plugin.³⁰

Hematoxylin and Eosin (HE) Staining

The histopathological evaluation of tissue sections was carried out using HE staining. Briefly, the tissues were immersed in 4% paraformaldehyde and fixed for 24h, dehydrated in 30% sucrose solution until the pathological tissue sank, embedded in OCT, and then cut into sections (8–10µm thick). After elution of OCT, tissue sections were first dyed with a hematoxylin solution for 5 min, then counter-stained with eosin for 2 min, and finally visualized by an optical microscope.

Real-Time Quantitative Reverse Transcriptions Polymerase Chain Reaction (RT-qPCR)

Total RNA of cells or tissues was extracted utilizing TRIzol reagent. RNA concentration was measured and reverse transcribed using Evo M-MLV Reverse Transcription PreMix Kit (Accurate Biology, Hunan, China). Subsequently, RT-qPCR was performed on a Bio-RAD real-time PCR system using SYBR Green Pro Taq HS PreMix Kit (Accurate Biology, Hunan, China) according to the manufacturer's instructions. The primer sequences were as follows: β-actin (human), F: 5'-GCCTCGCCTTTGCCGAT-3', R: 5'-CGCGGCGATATCATCATCCA-3'; IL-1β (human), F: 5'-AGCTACGAATCTCCGACCAC-3', R: 5'-CGTTATCCCATGTGTCGAAGAA-3'; IL-6 (human), F: 5'-CCTGAACCTTCCAAAGATGGC-3', R: 5'-TTCACCAGGCAAGTCTCCTCA-3'; IL-8 (human), F: 5'-ACTGAGAGTGATTGAGAGTGGAC-3', R: 5'-AACCCTCTGCACCCAGTTTTTC-3'; TNF-α (human), F: 5'-CCTCTCTCTAATCAGCCCTCTG-3', R: 5'-GAGGACCTGGAGTAGATGAG-3'. The relative mRNA expression levels of the target genes were calculated using the $2^{-\Delta\Delta Ct}$ method, with β-actin as the internal control for normalization.

Western Blotting

The cells or tissues were lysed in RIPA buffer for 30 min on ice to extract the total protein. Subsequently, the extracted protein was heated to 100°C for 5 min with loading buffer except for TRPV1, which was heated to 70°C for 5 min. The protein was then separated by 10%–12% SDS-PAGE gels and transferred to PVDF membranes. The membranes were then blocked using a rapid blocking buffer for 30 min under room temperature. Next, the membranes were immersed in primary antibodies overnight under 4°C. On the second day, the membranes were incubated with fluorescent secondary antibodies (goat anti-mouse or goat anti-rabbit) for 1h at room temperature. Finally, the membranes were washed three times using TBST, and the protein bands were detected through Image Studio Ver 4.0.

Immunofluorescence and Immunohistochemistry

For cell immunofluorescence analysis, RWPE-1 cells were seeded to 24-well plates with 1×10^4 cells per well. After drug treatment, the cells were gently washed with PBS three times. The cells were fixed with 4% paraformaldehyde for 30 min at room temperature, after which they were blocked with normal goat serum for 1h under 37°C. The RWPE-1 cells were then incubated with primary antibody overnight at 4°C. On a secondary day, the cells were stained with fluorescent secondary antibody for 1h at 37°C away from light. Finally, DAPI was added to each well for 5 min to visualize the nuclei. The fluorescent signal was captured using a fluorescence microscope. For tissue sections immunofluorescence analysis, after elution of OCT, permeated by 0.3% Triton X-100, blocked endogenous peroxidase, the sections were incubated with primary antibody overnight at 4°C. On the secondary day, the sections were stained with a fluorescent secondary antibody for 1h at 37°C away from light. Finally, DAPI was added to each well for 5 min to visualize the nuclei. The fluorescent signal was captured using a fluorescence microscope. The procedure of immunohistochemistry assay was roughly the same as that of immunofluorescence, except that DAB was used for color development on the second day after incubation of the secondary antibody. The nucleus was re-stained with hematoxylin. The sections were observed under a light microscope.

Surface Plasmon Resonance (SPR) Assay

The binding capacity *in vitro* between SERT and recombinant human TRPV1 protein (KMD Bioscience, Tianjin, China) was analyzed utilizing an SPR biosensor. TRPV1 protein was dissolved in sodium acetate (pH 4.0) at 70 μ g/mL and immobilized on the Carboxyl sensor chip (Nicoya, Canada). SERT was dissolved in PBS (pH 7.4) containing 1% DMSO. Different concentrations of SERT were injected into the sensor surface, and the analyte flow rate, association, and dissociation time were set as 20 μ L/min, 240s, and 360s respectively. SPR assay was performed on OpenSPR (Nicoya, Canada). Finally, the equilibrium dissociation constant (KD) was calculated to evaluate the binding affinity between SERT and TRPV1.

Statistical Analysis

All data were presented as mean \pm standard deviation (SD). Statistical analysis was conducted using GraphPad Prism 8.0.1. One-way ANOVA was used for the hypothesis test. For post hoc tests, comparisons among groups (all other groups compared to the LPS or EAP group) were predetermined. Dunnett's correction was used for multiple comparisons. $P < 0.05$ was regarded as statistically significant.

Results

The detailed workflow of this study is presented in Figure 1.

Potential Targets of SERT on CP

A total of 46 predicted targets related to SERT were obtained. The CP-related genes from GeneCards, DisGeNET, and OMIM databases were 4513, 20, and 25, respectively. A total of 4521 targets were obtained after combing all the results. There were 27 common targets between predicted targets of SERT and CP-related genes (Figure 2A). Then, we constructed the PPI network of the overlapped targets between SERT and CP. The network contained 25 nodes and 64 edges (Figure 2B). And the top 10 targets with the highest degree were also screened through Cytoscape. As HTR2B, TRPV1, SIGMAR1, CHRM1, ADRA1D, and ADRA1B had the same degree, a total of 14 proteins were present in the network (Figure 2C). Finally, we exhibited the degree of each protein in the PPI network (Figure 2D).

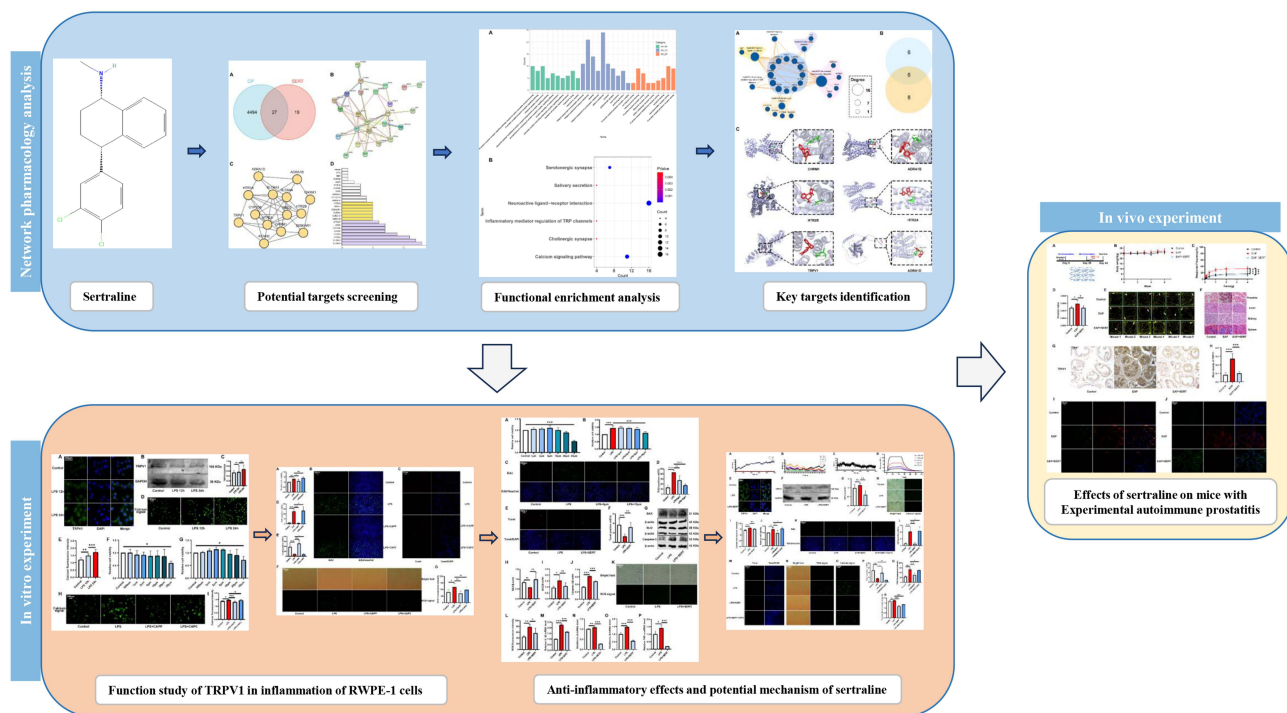


Figure 1 Schematic flowchart of the study strategy.

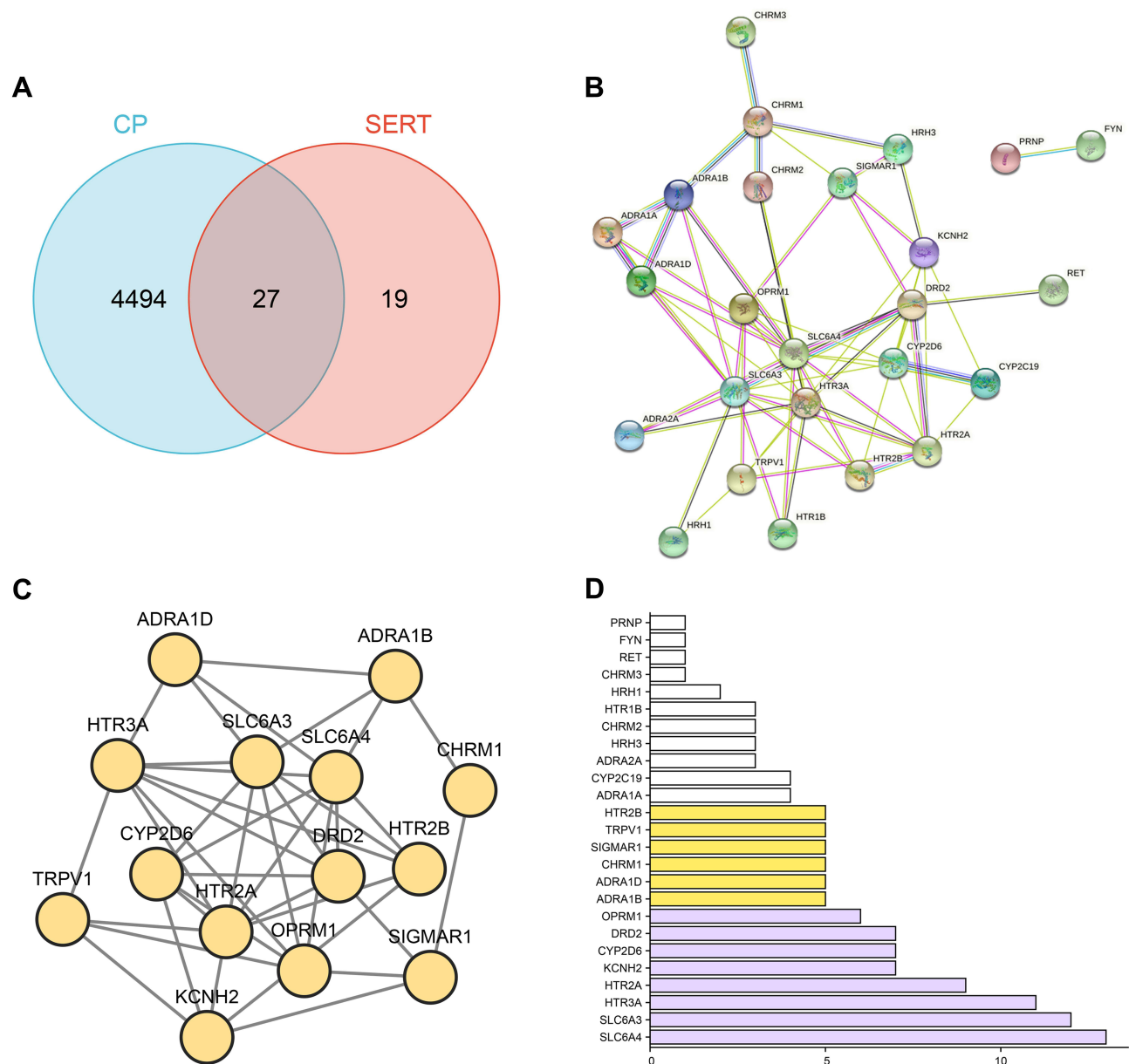


Figure 2 Prediction of potential targets of SERT on CP. (A) intersection of predicted targets of SERT and CP-related genes (B) PPI network of the overlapped targets between SERT and CP (C) the targets with the top 10 highest degrees in the PPI network (D) the degree of each target in the PPI network.

Go Enrichment and KEGG Pathway Analysis

The GO and KEGG function enrichment analysis of the common targets was conducted to discover the potential function of SERT on CP. A total of 31 biological processes (BP), 19 cell components (CC), and 9 molecular functions (MF) were enriched. We exhibited the 10 most significant results of each GO category in Figure 3A. And 6 KEGG pathways were obtained including neuroactive ligand–receptor interaction, calcium signaling pathway, serotonergic synapse, salivary secretion, inflammatory mediator regulation of TRP channels, and cholinergic synapse (Figure 3B).

Potentially Key Targets of SERT on CP

Firstly, the enriched pathways and predicted target of SERT contained in the pathways were imported to Cytoscape software. Then, the “target–pathway” network for SERT was constructed (Figure 4A). Twelve targets (HRH1, CHRM2, ADRA1A, CHRM1, HTR1B, HRH2, TRPV1, HTR2A, HTR2B, CHRM3, ADRA1D, and ADRA1B) were contained in at least two

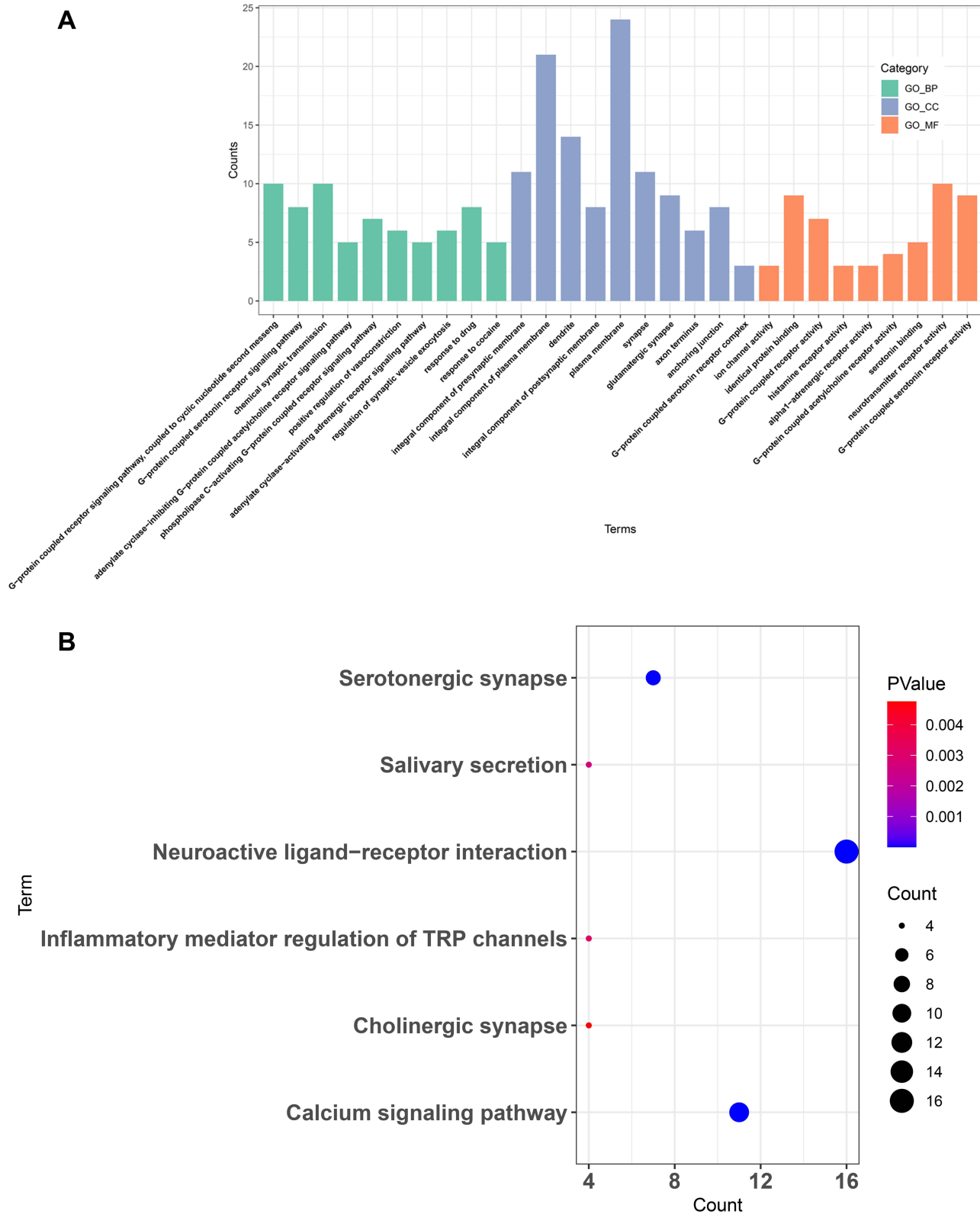


Figure 3 GO and KEGG functional enrichment analysis of the overlapped genes between predicted targets of SERT and CP-related genes. **(A)** GO functional enrichment analysis **(B)** KEGG functional enrichment analysis.

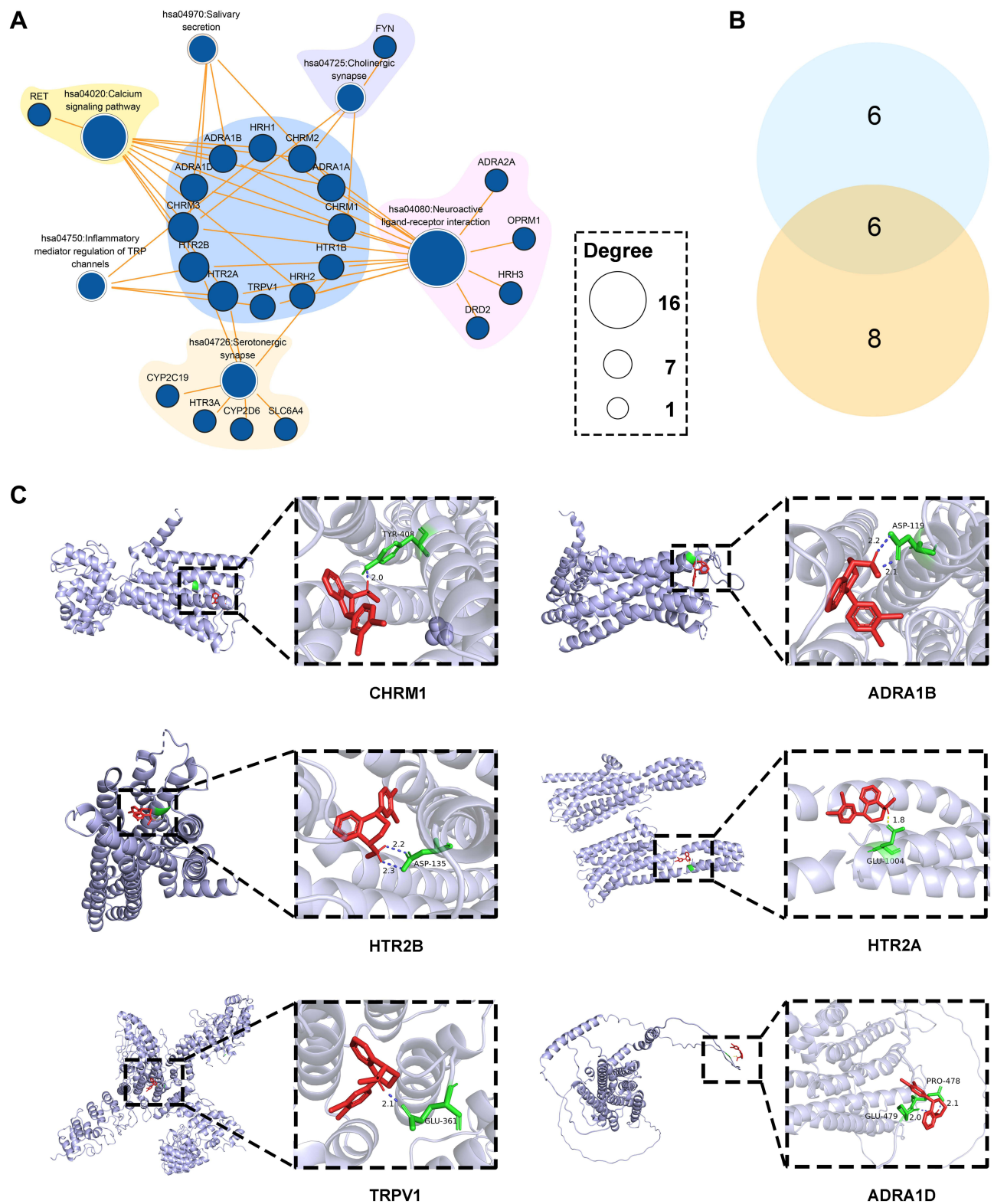


Figure 4 Identification of potentially key targets of SERT on CP. **(A)** the “target-pathway” network of SERT for CP **(B)** Venn diagram presented the intersection of key targets convolved in at least two pathways in the “target-pathway” network and key targets with relatively high degree values in the PPI network **(C)** molecular docking of SERT with potentially key targets of SERT on CP.

pathways. We took the intersection of the above 12 targets and the 14 proteins (SLC6A4, SLC6A3, HTR3A, HTR2A, KCNH2, CYP2D6, DRD2, OPRM1, ADRA1B, ADRA1D, CHRM1, SIGMAR1, TRPV1, and HTR2B) with relatively high degree values in the PPI network. Six common targets (CHRM1, TRPV1, HTR2A, HTR2B, ADRA1D, ADRA1B) were obtained which were considered as potentially key targets of SERT to treat CP by regulated multiple signal pathways (Figure 4B). Then, we conducted molecular docking for the 6 potentially key targets with SERT. The results showed that SERT docked well with CHRM1 (PDB ID: 6ZFZ, -8.33 kcal/mol), ADRA1B (PDB ID: 7B6W, -8.22 kcal/mol), HTR2B (PDB ID: 4IB4, -8.00 kcal/mol), HTR2A (PDB ID: 6A94, -6.81 kcal/mol), and TRPV1 (PDB ID: 6L93, -6.54 kcal/mol) (Figure 4C). Only the structure of ADRA1D was obtained from the AlphaFold Protein Structure Database (AlphaFold ID: AF-P25100-F1), and the affinity was -4.29 kcal/mol. To explore the mechanism of SERT to relieve the inflammation phenotype of RWPE-1 cells, we chose TRPV1 as the potential target because it was relatively central to the “target-pathway” network and TRPV1 had a relatively clear function in local inflammation of the prostate and CP-induced pain than any other potential targets.^{31–33}

Function of TRPV1 in the Inflammatory Phenotype of LPS-Stimulated RWPE-1 Cells

First, we evaluated the expression change of TRPV1 protein under LPS stimulation. Immunofluorescence and Western blot analysis indicated that LPS stimulation for 24h could elevate the expression of TRPV1 in RWPE-1 cells (Figure 5A–C). Then, to further explore the influence of LPS on the TRPV1 channel, intracellular calcium level was detected because one of the most important biological effects of TRPV1 activation was calcium influx.³⁴ It indicated that LPS could promote calcium influx of RWPE-1 cells, and the effect was more obvious with the prolongation of stimulation time (Figure 5D and E). Then, the antagonist (Capsazepine, CAPP) and agonist (Capsaicin, CAPC) of TRPV1 were utilized to explore the potential function of TRPV1. The cytotoxic effects of CAPP and CAPC on RWPE-1 cells were investigated via a CCK-8 kit. The results showed that 1–20 μ M CAPP or CAPC did not influence the vitality of RWPE-1 cells (Figure 5F and G). Therefore, 10 μ M CAPP or CAPC was adopted in the subsequent experiments. Intracellular calcium signal detection suggested that CAPP could inhibit calcium influx, while CAPC pretreatment had no significant difference on calcium influx with LPS-stimulated RWPE-1 cells (Figure 5H and I).

We then evaluated the influence of CAPP and CAPC on the proliferation of LPS-stimulated RWPE-1 cells. CCK-8 assay showed that LPS could promote the proliferation of RWPE-1 cells, and CAPP could inhibit this effect, while CAPC preconditioning had no significant effect on LPS-stimulated RWPE-1 proliferation (Figure 6A). The results of EdU assay also confirmed this (Figure 6B and D). A tunnel assay was utilized to assess the impact of CAPP and CAPC on the apoptosis process of LPS-stimulated RWPE-1 cells. The results showed that Tunel⁺ cells significantly decreased in LPS-stimulated RWPE-1 cells indicating apoptosis inhibition due to LPS stimulation. Tunel⁺ cells in RWPE-1 cells receiving CAPP were significantly elevated, suggesting that CAPP could alleviate apoptosis inhibition induced by LPS stimulation. CAPC preconditioning had no significant effect on LPS-stimulated RWPE-1 apoptosis inhibition (Figure 6C and E). To evaluate the influence of CAPP and CAPC on the oxidative stress of LPS-stimulated RWPE-1 cells, we detected the ROS level in RWPE-1 cells. It suggested that LPS could significantly improve the generation of ROS in RWPE-1 cells, and CAPP significantly inhibited such effects, while CAPC pretreatment had no significant difference with LPS-stimulated RWPE-1 cells (Figure 6F and G).

Effects of SERT on the Inflammatory Phenotype of LPS-Induced RWPE-1 Cells

Firstly, we explore the cytotoxic effect of various concentrations of SERT on RWPE-1 cells via a CCK-8 kit. We found 1–20 μ M SERT did not influence the vitality of RWPE-1 cells (Figure 7A). Then, the effects of different concentrations (1 μ M, 2 μ M, 5 μ M, and 10 μ M) of SERT on LPS-stimulated RWPE-1 cells were also explored via CCK-8 assay. We found SERT could inhibit the proliferation of LPS-stimulated RWPE-1 cells in a dose-dependent manner (Figure 7B). Additionally, we also performed an EdU assay to assess the influence of SERT (5 μ M and 10 μ M) on cell proliferation of LPS-stimulated RWPE-1 cells. EdU-positive RWPE-1 cells were significantly improved after LPS stimulation, while SERT pre-treatment could significantly eliminate this change (Figure 7C and D). Then, 10 μ M SERT was adopted for subsequent experiments. We evaluated the influence of SERT on apoptosis inhibition of RWPE-1 cells after LPS stimulation utilizing Tunel assay. The results showed that SERT could significantly increase the amount of Tunel⁺ cells indicating that SERT could alleviate apoptosis inhibition induced by LPS stimulation (Figure 7E and F). We also detected the expression level of three apoptosis-related regulatory proteins (Figure 7G–J).

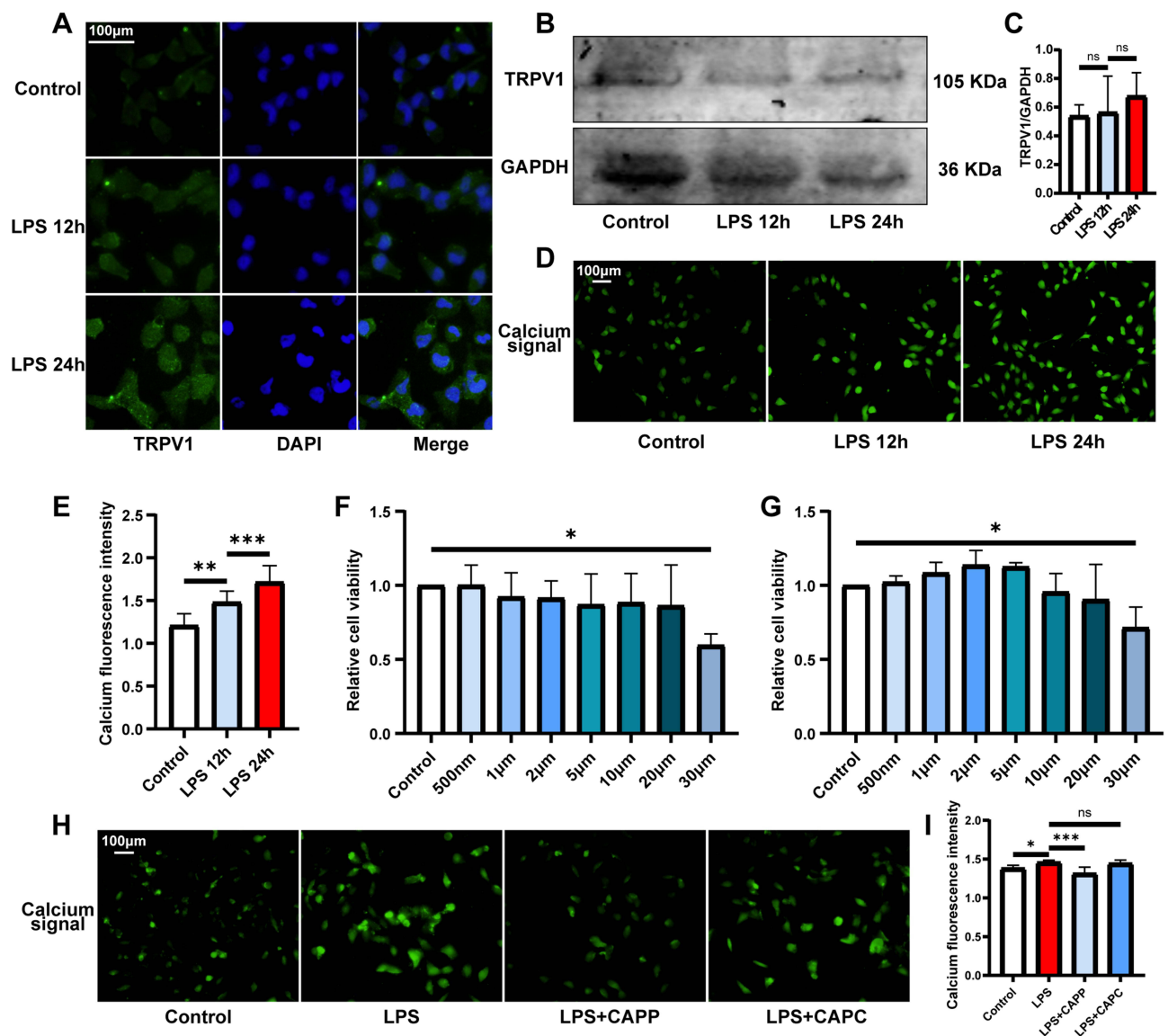


Figure 5 Changes in the expression and function of TRPV1 under LPS stimulation. (A) immunofluorescence staining of TRPV1 in RWPE-1 cells under LPS stimulation (B) Western blot analysis of expression of TRPV1 in RWPE-1 cells under LPS stimulation (C) quantitative statistics of expression differences of Western blot analysis of TRPV1 (D) intracellular calcium imaging of RWPE-1 cells under LPS stimulation (E) quantitative statistics of intracellular calcium level of RWPE-1 cells under different treatments (F) the toxicity of different CAPP concentrations on RWPE-1 cells via CCK-8 assay (G) the toxicity of different CAPC concentrations on RWPE-1 cells via CCK-8 assay (H) intracellular calcium imaging of RWPE-1 cells under different treatments (I) quantitative statistics of intracellular calcium level of RWPE-1 cells under different treatments. ns: $P > 0.05$, * $P < 0.05$, ** $P < 0.01$, *** $P < 0.001$.

LPS could inhibit the expression of BAX in RWPE-1 cells, and elevate the expression of Bcl2 and Caspase-3. Pretreatment of SERT could reduce the effect of LPS on the expression of apoptotic proteins in RWPE-1 cells. To evaluate the influence of SERT on the oxidative stress of LPS-stimulated RWPE-1 cells, we detected the ROS level in RWPE-1 cells. It suggested that LPS could significantly improve the generation of ROS in RWPE-1 cells, while SERT pretreatment significantly inhibited such an effect (Figure 7K and L). Finally, four inflammatory cytokines (IL-1 β , IL-6, IL-8, TNF- α) were detected utilizing RT-qPCR (Figure 7M-P). LPS significantly elevated the transcriptional level of the four cytokines, while SERT pretreatment significantly down-regulated the transcription level of these inflammatory cytokines.

Effect of SERT on TRPV1 Channel

Firstly, to further examine the binding stability of SERT with TRPV1, an MD simulation was conducted (Figure 8A-C). The RMSD curve indicated that the protein-ligand was stable in the late simulation period (Figure 8A). The RMSF and Rg values

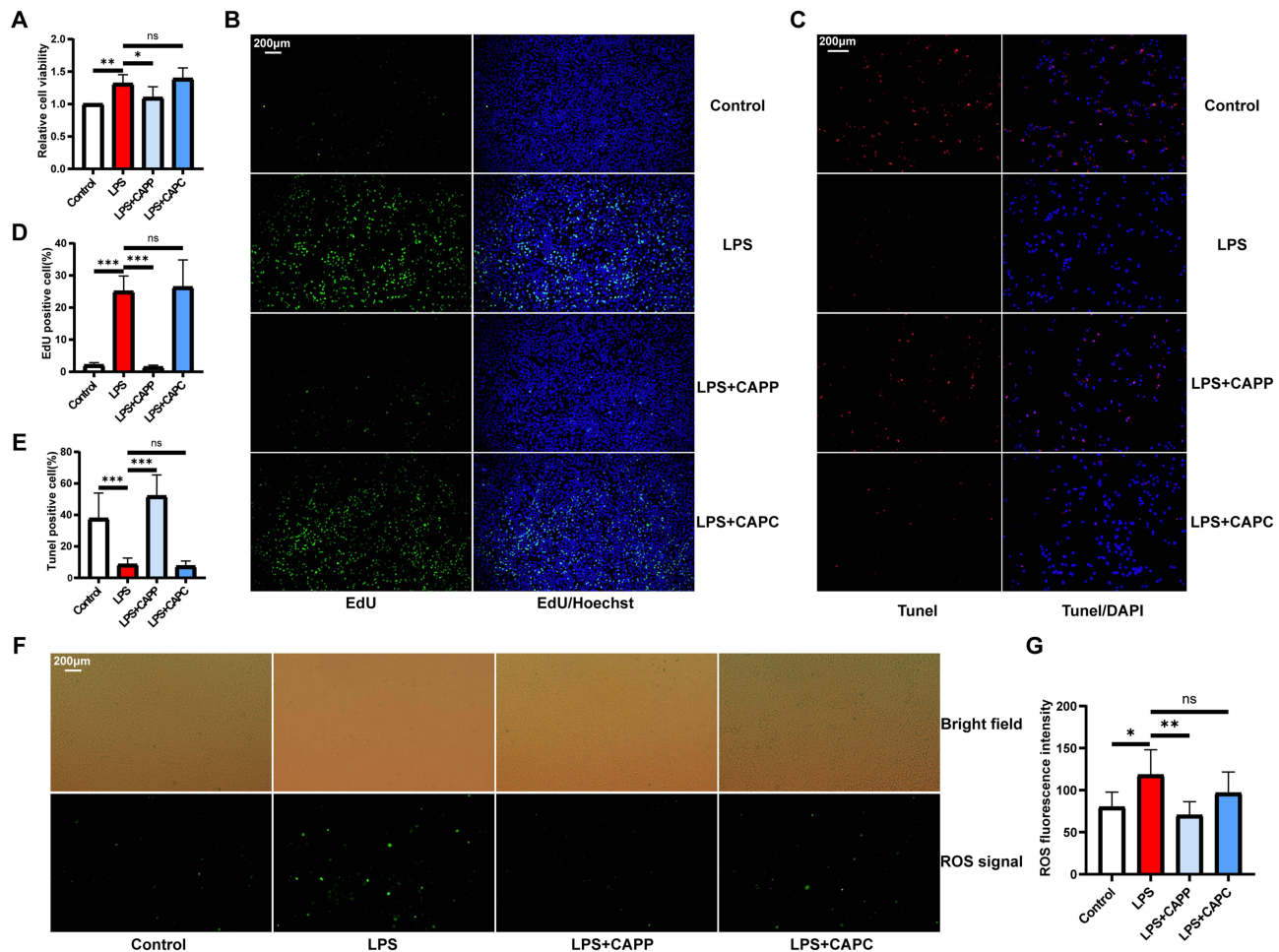


Figure 6 Function exploration of TRPV1 in LPS-stimulated RWPE-1 cell. (A) the effects of CAPP and CAPC on the proliferation of LPS-stimulated RWPE-1 cells via CCK-8 assay (B) the effects of CAPP and CAPC on the proliferation of LPS-stimulated RWPE-1 cells via EdU assay (C) the effects of CAPP and CAPC on the apoptosis process of LPS-stimulated RWPE-1 cells via TUNEL assay (D) quantitative analysis of EdU assay (E) quantitative analysis of TUNEL assay (F) the effects of CAPP and CAPC on ROS generation of LPS-stimulated RWPE-1 cells via fluorescence detection of DCFH-DA probe (G) quantitative analysis of fluorescence intensity of DCFH-DA probe. ns: $P > 0.05$, * $P < 0.05$, ** $P < 0.01$, *** $P < 0.001$.

indicated that the protein gradually became more stable as the MD simulation progressed (Figure 8B and C). The binding free energy was calculated as -9.48kcal/mol . Then, SPR assay was performed, and the binding capacity of SERT to TRPV1 in vitro was confirmed (Figure 8D). The KD value was calculated as $91.8\mu\text{M}$. Immunofluorescence and Western blot analysis of the expression of TRPV1 protein in RWPE-1 cells with different treatments were also performed (Figure 8E–G). LPS could slightly elevate the expression of TRPV1 in RWPE-1 cells, and SERT pre-treatment could significantly down-regulate the expression of TRPV1. It indicated that LPS could induce calcium influx of RWPE-1 cells, and SERT pre-treatment could suppress such effect (Figure 8H and I). Next, we evaluated whether CAPC could rescue the anti-inflammatory effects of SERT for LPS-stimulated RWPE-1 cells. CCK-8 assay confirmed that CAPC could rescue the antiproliferative effect of SERT for LPS-stimulated RWPE-1 cells (Figure 8J). The results of EdU assay also confirmed this (Figure 8K and L). Furthermore, through the TUNEL assay, ROS signal detection, and calcium signal evaluation, we found the rescue effects of CAPC on the function of SERT in promoting apoptosis (Figure 8M and P), inhibiting ROS production (Figure 8N and Q), and inhibiting calcium influx (Figure 8O and R) of LPS-stimulated RWPE-1 cells, respectively.

Effects of SERT on EAP Mice

To further clarify the efficacy and mechanism of SERT in the treatment of CP, in vivo experiments based on EAP mice model were conducted. The flow chart of the animal experiment is presented in Figure 9A. The body weight changes of

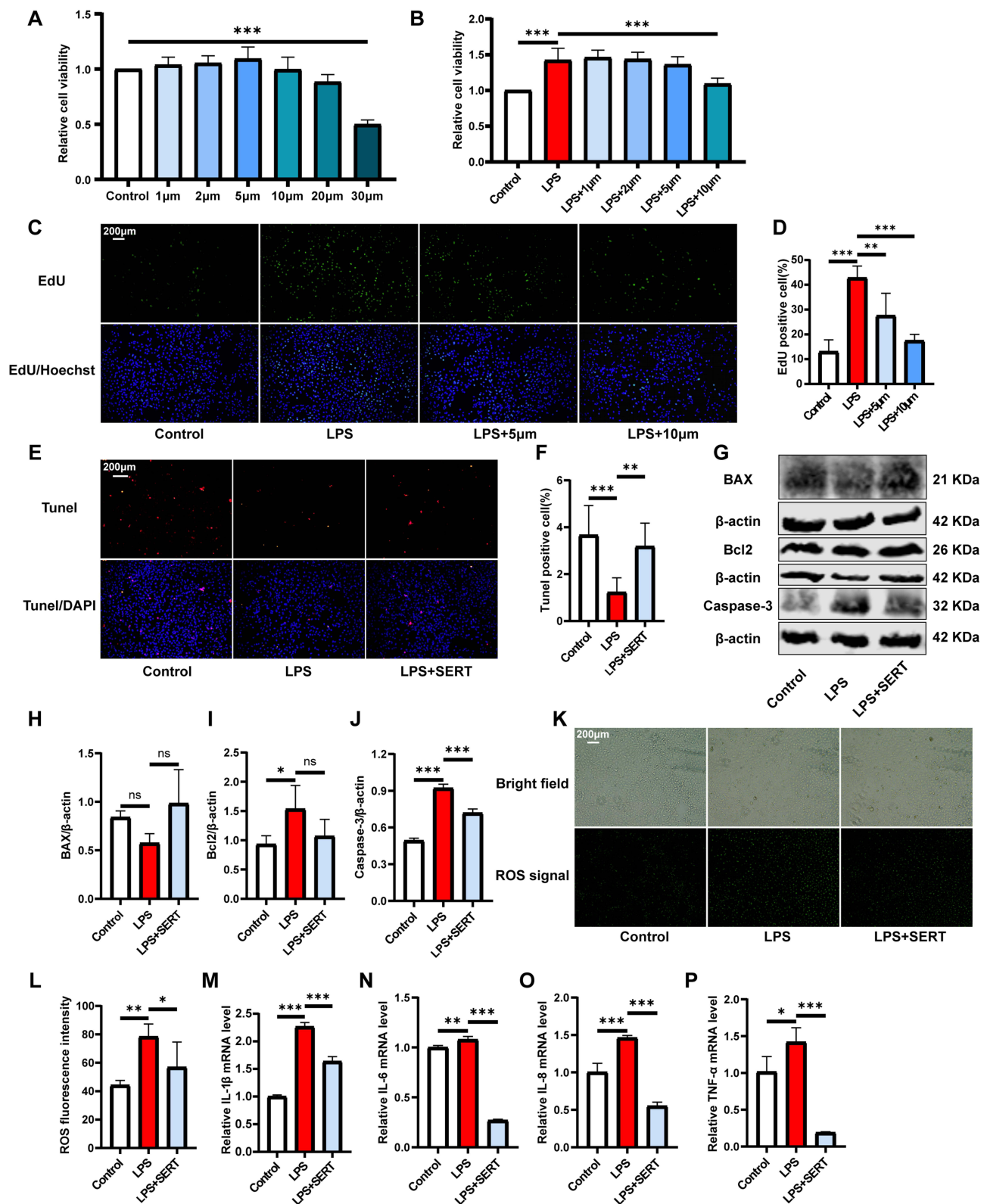


Figure 7 The anti-inflammation effects of SERT for LPS-stimulated RWPE-1 cells. **(A)** the toxicity of different SERT concentrations on RWPE-1 cells via CCK-8 assay **(B)** the anti-proliferation effect of different SERT concentrations on LPS-stimulated RWPE-1 cells via CCK-8 assay; **(C)** the anti-proliferation effect of SERT on LPS-stimulated RWPE-1 cells via EdU assay; **(D)** quantitative analysis of EdU assay **(E)** the effects of SERT on the apoptosis process of LPS-stimulated RWPE-1 cells via TUNEL assay **(F)** quantitative analysis of TUNEL assay **(G)** Western blot analysis of apoptosis-related proteins (BAX, Bcl2, and Caspase-3) **(H-J)** quantitative statistics of expression differences of apoptosis-related proteins under different treatments **(H):** BAX, **I:** Bcl2, **J:** Caspase-3 **(K)** the effect of SERT on ROS generation via fluorescence detection of DCFH-DA probe **(L)** quantitative analysis of fluorescence intensity of DCFH-DA probe; **(M-P):** RT-qPCR evaluated the level of inflammatory cytokines **(M):** IL-1β, **N:** IL-6, **O:** IL-8, **P:** TNF-α. ns: P>0.05, *P<0.05, **P<0.01, ***P<0.001.

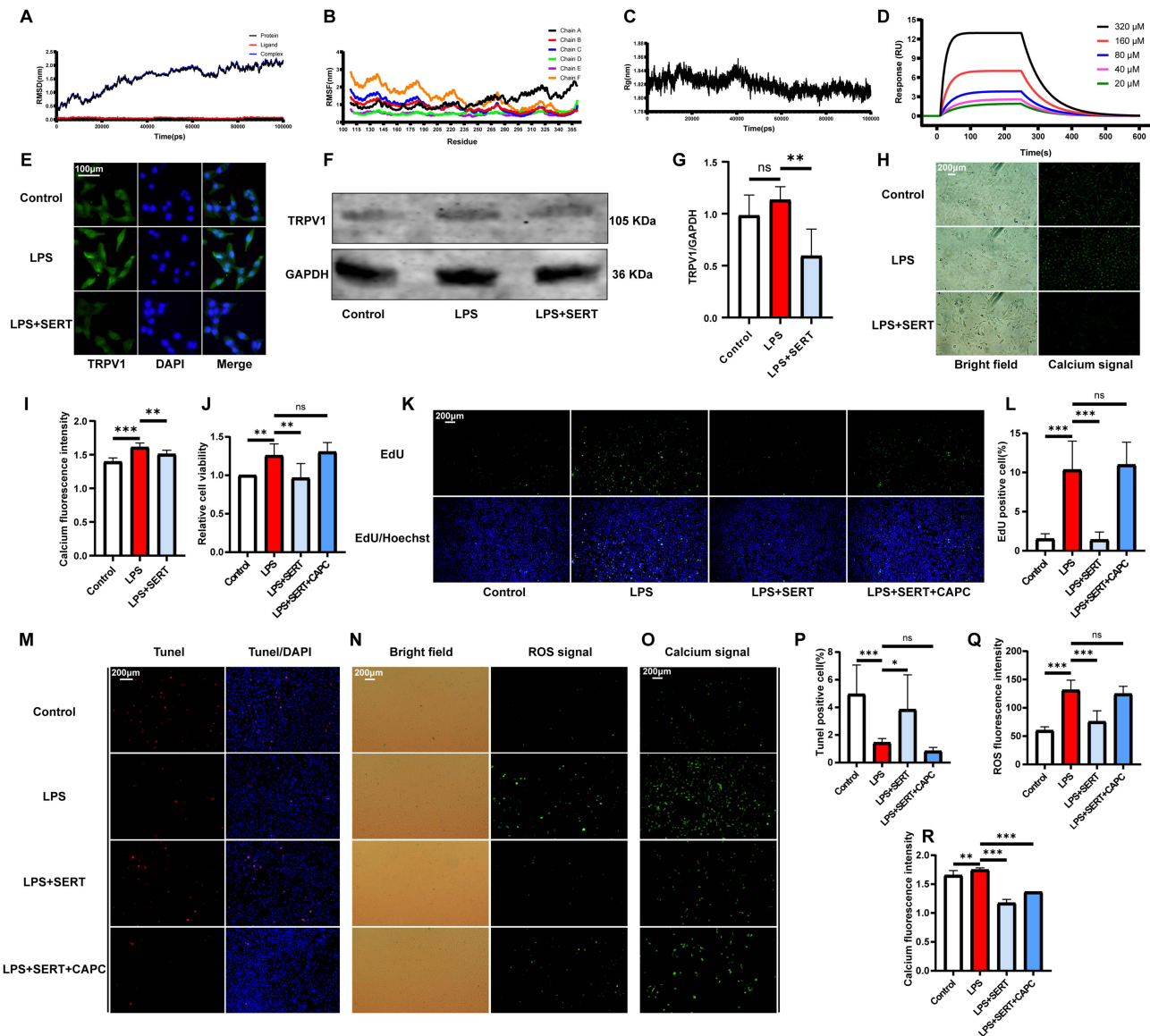


Figure 8 Effect of SERT on TRPV1 channel in RWPE-1 cells. (A–C) MD simulation of SERT-TRPV1 complex (D) SPR assay for the binding capacity of SERT with TRPV1 in vitro (E) immunofluorescence staining of TRPV1 in RWPE-1 cells under different treatments (F) Western blot analysis of expression of TRPV1 in RWPE-1 cells under different treatments (G) quantitative statistics of expression differences of Western blot analysis of TRPV1 (H) intracellular calcium imaging of RWPE-1 cells under different treatments (I) quantitative statistics of intracellular calcium level of RWPE-1 cells under different treatments (J) rescue effect of CAPC on anti-proliferative effect of SERT for LPS-stimulated RWPE-1 cells via CCK-8 assay (K) rescue effect of CAPC on anti-proliferative effect of SERT for LPS-stimulated RWPE-1 cells via EdU assay (L) quantitative analysis of EdU assay (M) rescue effect of CAPC on SERT in promoting apoptosis of LPS-stimulated RWPE-1 cells via TUNEL assay (N) rescue effect of CAPC on anti-ROS effect of SERT for LPS-stimulated RWPE-1 cells via fluorescence detection of DCFH-DA probe (O) rescue effect of CAPC on anti-calcium influx effect of SERT for LPS-stimulated RWPE-1 via intracellular calcium imaging (P) quantitative analysis of TUNEL assay (Q) quantitative analysis of fluorescence intensity of DCFH-DA probe (R) quantitative statistics of intracellular calcium level of RWPE-1 cells under different treatments. ns: $P > 0.05$, $*P < 0.05$, $**P < 0.01$, $***P < 0.001$.

mice during the experiment are shown in Figure 9B. As shown in Figure 9C, EAP mice behaved with a more positive pain response than the control mice, while SERT treatment could relieve the abnormal pain response. The prostate index of EAP mice was significantly higher than that of control mice, and SERT treatment could reduce the prostate index of EAP mice (Figure 9D). Results of the open-field test suggested that EAP mice exhibited reduced spontaneous exploratory activity, indicating depressive-like behavior of EAP mice, and the symptom was alleviated by SERT treatment (Figure 9E). HE staining of prostates suggested prostatic inflammation in EAP mice, while SERT treatment could reduce the prostatic inflammation in EAP mice (Figure 9F). In addition, HE staining of the liver, spleen, and kidney of the mice did not show any significant abnormality, indicating that SERT had no significant toxic effects on mice liver,

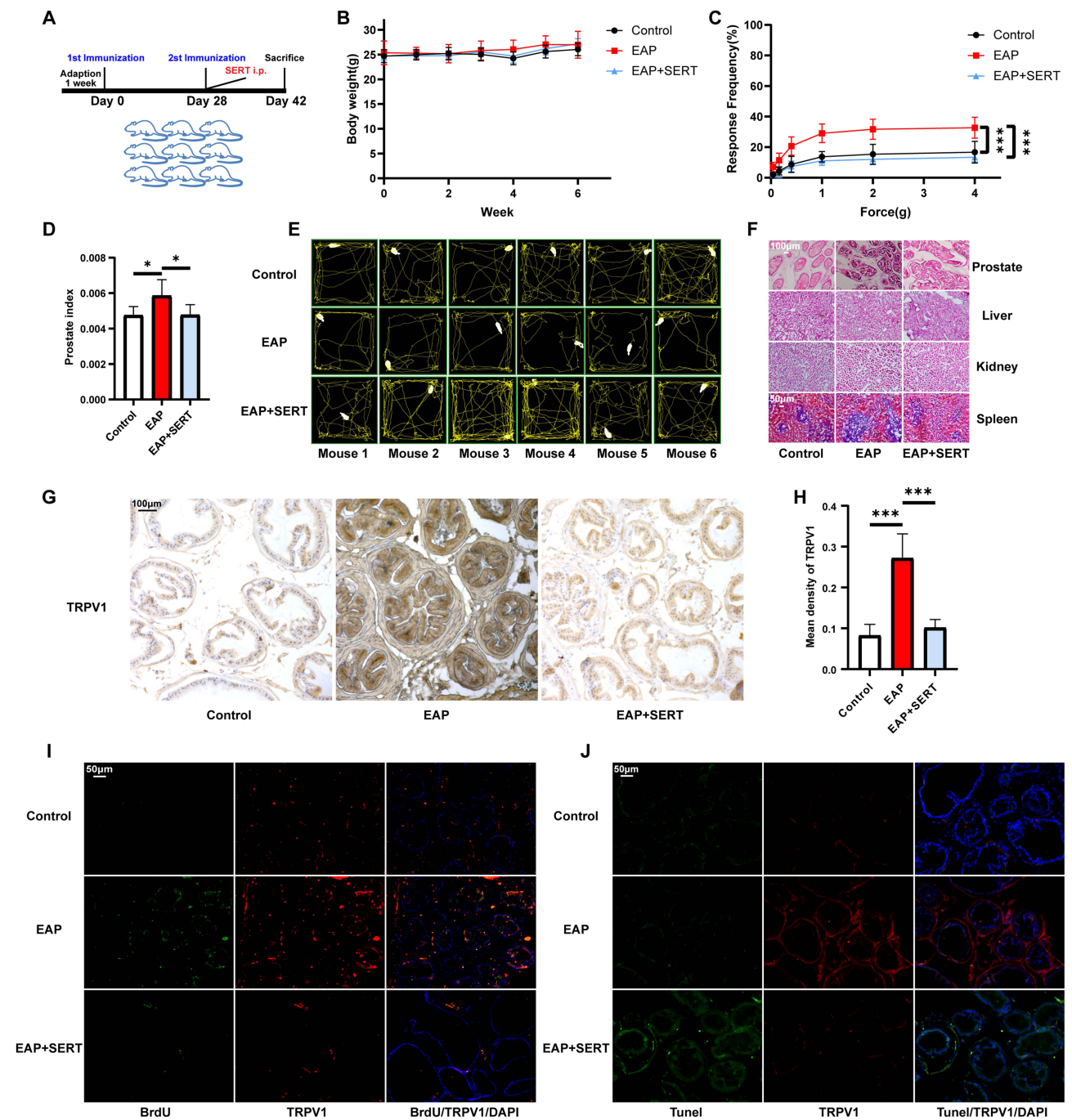


Figure 9 To explore the effect and mechanism of SERT for CP in EAP mice. (A) schematic diagram of mice experiment procedure (B) body weight changes of mice in each group (C) results of von Frey filaments test for pain response of mice in each group at the end of the experiment (D) prostate index of mice in each group (E) results of open-field tests for depressive-like symptoms of mice in each group at the end of the experiment (F) histopathological evaluation of prostate, liver, kidney, and spleen of mice in each group (G) immunohistochemical analysis of the expression of TRPV1 in the prostate of mice in each group (H) quantitative statistics of immunohistochemical analysis (I) immunofluorescence double staining of BrdU/TRPV1 of the prostate sections of mice in each group; (J) immunofluorescence double staining of TUNEL/TRPV1 of the prostate sections of mice in each group. * $P < 0.05$, *** $P < 0.001$.

kidney, and spleen under the present experimental conditions (Figure 9F). Then, immunohistochemical staining was utilized to evaluate the expression of TRPV1 in prostate tissues of the mice. TRPV1 was significantly highly expressed when compared with the control group. After the treatment of SERT, the expression of TRPV1 was significantly down-regulated (Figure 9G and 9H). Furthermore, based on immunofluorescence staining, we found that the prostate tissues of EAP mice showed more BrdU⁺ cells indicating abnormal proliferation, while SERT treatment could inhibit the

proliferation (Figure 9I). Finally, Tunel assay suggested that there seemed to be no significant difference in Tunel⁺ cells in the prostate tissues between EAP mice and control mice, but SERT treatment could significantly increase Tunel⁺ cells in the prostate tissues indicating that SERT could promote apoptosis of the prostate tissues of EAP mice (Figure 9J).

Discussion

CP is one of the most significant clinical challenges within our urology department because of its enormously increasing incidence, damage to the quality of life, heterogeneous clinical symptoms, and subpar efficacy.³⁵ New treatment options are currently sorely needed. Although SERT has been widely used for the treatment of CP, the use scenarios and conditions are often unclear. Whether to prescribe SERT to CP patients without psychosomatic symptoms remains a problem for clinicians. Interestingly, current clinical trials focusing on SERT for the treatment of CP often did not specifically distinguish between psychiatric symptoms in the patients.⁹ In this study, we have discovered the anti-inflammation effect of SERT on LPS-stimulated RWPE-1 cells and prostatic inflammation of EAP mice, while the potential mechanism is regulating the TRPV1 channel. Our results might standardize and extend the application scenario of SERT in the treatment of CP. That is, it might be not only suitable for CP patients with depressive symptoms but for anyone diagnosed with CP.

LPS-induced RWPE-1 cells were proven to simulate the pathological features of chronic nonbacterial prostatitis (CNP).^{36–38} Thus, LPS-induced RWPE-1 cells were used as the *in vitro* model for our study. 10 μ g/mL LPS stimulation for 24h was found to promote the proliferation, ROS generation, transcription of inflammatory cytokines, and inhibited the apoptosis of RWPE-1 cells, which were consistent with previous studies.^{36,39,40} We discovered that SERT could suppress the proliferation, ROS generation, transcription of inflammation cytokines and promote the apoptosis of LPS-induced RWPE-1 cells. It indicated that SERT could relieve the inflammatory response of LPS-stimulated RWPE-1 cells. Furthermore, EAP mice model, a common *in vivo* model for CP,^{27,41} was built to further explore the effect and mechanism of SERT on CP. Our data confirmed that SERT treatment could reduce pain response, improve depression-like symptoms, relieve local prostate inflammation, inhibit the proliferation and promote apoptosis of prostate tissues in EAP mice. These results suggested that SERT might not only treat CP by affecting mental state but also act directly to exert anti-inflammatory effects locally. Notably, whether *in vitro* or *in vivo* models, there seemed to be contradictions about the apoptosis process in the previous literature. Song et al found that the apoptosis process of RWPE-1 cells was significantly inhibited by LPS,³⁶ while Sun et al reported that LPS stimulation promoted the apoptosis of RWPE-1 cells.⁴² Similarly, the changes in the apoptosis process were also inconsistent with EAP mice model in previous literature.^{41,43} Our previous review has discussed such inconsistencies.⁴⁴ The potential reasons might be internal differences in the models, such as different types of mice used to build the EAP model, or heterogeneity of the detection process that should be further explored in the future. However, considering other indicators, we still have reason to infer the anti-inflammatory effect of SERT for CP.

Network pharmacological analysis and molecular docking were used to predict the potential anti-inflammatory mechanism of SERT in our study. TRPV1 was finally identified as a vital target of SERT. At the end of the 1990s, TRPV1, transient receptor potential vanilloid 1, was identified to serve as a key sensor of pain and heat in humans.⁴⁵ So far, TRPV1 has been confirmed to be linked to the process of inflammation, immunity, and cancer, and was validated as a therapeutic target in multiple preclinical models of chronic pain, including cancer, neuropathic, postoperative, and musculoskeletal pain.^{46,47} In this study, we confirmed the regulatory role of SERT on the expression and function of TRPV1 in RWPE-1 cells by MD simulation, SPR assay, immunofluorescence, Western blot, and calcium imaging. Functional experiments indicated that TRPV1 held an important role in LPS-induced RWPE-1 proliferation, apoptosis, and oxidative stress processes. Combined with the rescue experiments of the anti-inflammatory phenotype of SERT based on TRPV1 agonist (CAPC), we deduced that the anti-inflammatory effects of SERT might be mediated by the expression and function of TRPV1. TRPV1 channel was found to be vital to persistent pelvic tactile allodynia while regulating TRPV1 in the prostate might be a promising strategy to relieve chronic pelvic pain.³³ It showed that TRPV1 knockout suppressed mast cell activity in the prostate of rats with experimental autoimmune prostatitis (EAP).³³ The mast cell-tryptase-PAR2 axis was previously reported to have a critical role in the development of chronic pelvic pain, while mast cell-directed therapy showed a promising effect in improving symptoms and regulating the immune inflammatory environment of CP patients.^{48,49} This suggests that the regulatory mechanism of TRPV1 in prostatitis

may be to improve the inflammatory cell infiltration and immune microenvironment of the prostate. Although TRPV1 was found to be up-regulated in the prostate tissues of EAP animals,^{31,50} the molecular mechanism of TRPV1 in the regulation of prostatic inflammation was rarely explored. Some studies have reported that TRPV1 plays a crucial role in the regulation of proinflammatory STAT3 signaling.^{51,52} IL-6/STAT3 pathway was also found to be involved in the regulation of chronic non-bacterial prostatitis,⁵³ suggesting that TRPV1 might participate in the inflammatory molecular interaction network of prostatic inflammation to regulate the occurrence and development of CP. Zhang et al found elevated expression of TRPV1 both in the prostate, bladder, and spinal dorsal root ganglion (DRG) in EAP rats.³¹ This demonstrated the potential of SERT to act as a regulator for TRPV1 at various sites, not only the prostate, to relieve chronic pelvic pain in CP patients.

In this study, we have discovered the anti-inflammatory effect of SERT on LPS-induced RWPE-1 cells and EAP mice, and the potential anti-inflammation mechanism is to regulate the TRPV1 channel. To our knowledge, this is the first report on the direct anti-inflammatory effect and potential mechanism of SERT for CP. The results promote us to re-examine the indications for SERT in CP patients. SERT may not only be used in CP patients with depressive symptoms but might also be used as a complementary anti-inflammatory agent for all CP patients. Our previous network meta-analysis evaluating the efficacy and safety of SSRIs in CP found that many clinical studies did not distinguish psychiatric symptoms in patients with CP.⁹ In order to further clarify the clinical scenarios of SERT treatment for CP, future clinical studies need to distinguish the psychiatric symptoms in CP patients to further clarify the efficacy difference of SERT in CP patients with and without psychiatric symptoms. At the same time, this highlights the importance of recognizing psychiatric symptoms in the clinical care of CP patients. However, there are some limitations to our study. Firstly, only RWPE-1 cells were adopted as the *in vitro* model. Although the cells are also used in many studies, and due to the pathophysiological complexity of CP, stromal cell lines of prostate such as WPMY-1 should also be further studied to verify our results. Secondly, TRPV1 has been found to play an important role in inflammation and pain, but the mechanism by which TRPV1 regulates CP is unclear. Although SERT was found to modulate TRPV1 to improve CP, the downstream mechanism of TRPV1 still needs to be further elucidated. Thirdly, network pharmacological strategies were used to discover potential mechanisms of SERT for CP in this study, which might have led to the neglect of other mechanisms, and additional mechanisms of SERT for CP should be explored in the future.

Conclusion

In conclusion, we have demonstrated that SERT has a significant anti-inflammatory effect on LPS-induced RWPE-1 cells and EAP mice. SERT inhibited cell proliferation, ROS generation, and transcription of inflammatory cytokines and promoted cell apoptosis of LPS-induced RWPE-1 cells. Additionally, SERT treatment could reduce pain response, improve depression-like symptoms, relieve local prostate inflammation, inhibit the proliferation and promote apoptosis of prostate tissues in EAP mice. The potential anti-inflammation mechanism of SERT for CP was down-regulating the expression and inhibiting the function of the TRPV1 channel. It indicated that SERT might serve as a complementary anti-inflammatory agent for CP.

Data Sharing Statement

If needed, the original data can be obtained by contacting the corresponding author.

Acknowledgments

This work was supported by the National Natural Science Foundation of China (Grant No. 82160148) and the Cuiying Scientific Training Program for Undergraduates of Lanzhou University Second Hospital (Grant No. CYXZ2021-16 and CYXZ2022-41). The funders had no role in the study design, experiment process, analysis, decision to publish, or preparation of the manuscript.

Author Contributions

The study was proposed and designed by Yongfeng Lao and Zhilong Dong. All authors made a significant contribution to the execution, data acquisition, analysis and interpretation of the study. The manuscript was drafted by Yongfeng Lao and

Zhilong Dong. All the authors took part in revising or critically reviewing the article; gave final approval of the version to be published; have agreed on the journal to which the article has been submitted; and agree to be accountable for all aspects of the work.

Disclosure

The authors declare no conflict of interest, financial or otherwise in this work.

References

1. Rees J, Abrahams M, Doble A, et al. Diagnosis and treatment of chronic bacterial prostatitis and chronic prostatitis/chronic pelvic pain syndrome: a consensus guideline. *BJU Int.* 2015;116(4):509–525. doi:10.1111/bju.13101
2. Krieger JN, Lee SWH, Jeon J, et al. Epidemiology of prostatitis. *Int J Antimicrob Agents.* 2008;31(1):S85–90. doi:10.1016/j.ijantimicag.2007.08.028
3. Healy R, Thorne C, Manjunath A. Chronic prostatitis (chronic pelvic pain syndrome). *BMJ.* 2023;383:e073908. doi:10.1136/bmj-2023-073908
4. Pena VN, Engel N, Gabrielson AT, et al. Diagnostic and management strategies for patients with chronic prostatitis and chronic pelvic pain syndrome. *Drugs Aging.* 2021;38(10):845–886. doi:10.1007/s40266-021-00890-2
5. Magistro G, Wagenlehner FME, Grabe M, et al. Contemporary management of chronic prostatitis/chronic pelvic pain syndrome. *Eur Urol.* 2016;69(2):286–297. doi:10.1016/j.eururo.2015.08.061
6. Chung SD, Huang CC, Lin HC. Chronic prostatitis and depressive disorder: a three year population-based study. *J Affect Disord.* 2011;134(1–3):404–409. doi:10.1016/j.jad.2011.05.046
7. Lien CS, Chung C-J, Lin C-L, et al. Increased risk of prostatitis in male patients with depression. *World J Biol Psychiatry.* 2020;21(2):111–118. doi:10.1080/15622975.2018.1533994
8. Barone B, De Luca L, Napolitano L, et al. Lower urinary tract symptoms and mental health during COVID-19 pandemic. *Arch Ital Urol Androl.* 2022;94(1):46–50. doi:10.4081/aiau.2022.1.46
9. Lao Y, He L, Zhang P, et al. Efficacy and safety of selective serotonin reuptake inhibitors for chronic prostatitis/chronic pelvic pain syndrome: a systematic review and network meta-analysis. *Asian J Surg.* 2022. 2810–2812. doi:10.1016/j.asjsur.2022.06.047
10. Harkin A, Kelly JP, McNamara M, et al. Activity and onset of action of reboxetine and effect of combination with sertraline in an animal model of depression. *Eur J Pharmacol.* 1999;364(2–3):123–132. doi:10.1016/S0014-2999(98)00838-3
11. Kim S, Chen J, Cheng T, et al. PubChem 2019 update: improved access to chemical data. *Nucleic Acids Res.* 2019;47(D1):D1102–d1109. doi:10.1093/nar/gky1033
12. Daina A, Michielin O, Zoete V. SwissTargetPrediction: updated data and new features for efficient prediction of protein targets of small molecules. *Nucleic Acids Res.* 2019;47(W1):W357–w364. doi:10.1093/nar/gkz382
13. Stelzer G, Rosen N, Plaschkes I, et al. The geneCards suite: from gene data mining to disease genome sequence analyses. *Curr Protoc Bioinform.* 2016;54:1.30.1–1.30.33. doi:10.1002/cpbi.5
14. Piñero J, Queralt-Rosinach N, Bravo A, et al. DisGeNET: a discovery platform for the dynamical exploration of human diseases and their genes. *Database.* 2015;2015:bav028. doi:10.1093/database/bav028
15. Amberger JS, Bocchini CA, Scott AF, et al. OMIM.org: leveraging knowledge across phenotype-gene relationships. *Nucleic Acids Res.* 2019;47(D1):D1038–d1043. doi:10.1093/nar/gky1151
16. von Mering C. STRING: known and predicted protein-protein associations, integrated and transferred across organisms. *Nucleic Acids Res.* 2005;33(Database issue):D433–7. doi:10.1093/nar/gki005
17. Sherman BT, Hao M, Qiu J, et al. DAVID: a web server for functional enrichment analysis and functional annotation of gene lists (2021 update). *Nucleic Acids Res.* 2022;50(W1):W216–21. doi:10.1093/nar/gkac194
18. Burley SK, Bhikadiya C, Bi C, et al. RCSB protein data bank: Powerful new tools for exploring 3D structures of biological macromolecules for basic and applied research and education in fundamental biology, biomedicine, biotechnology, bioengineering and energy sciences. *Nucleic Acids Res.* 2021;49(D1):D437–d451. doi:10.1093/nar/gkaa1038
19. Jumper J, Evans R, Pritzel A, et al. Highly accurate protein structure prediction with AlphaFold. *Nature.* 2021;596(7873):583–589. doi:10.1038/s41586-021-03819-2
20. Varadi M, Anyango S, Deshpande M, et al. AlphaFold protein structure database: Massively expanding the structural coverage of protein-sequence space with high-accuracy models. *Nucleic Acids Res.* 2022;50(D1):D439–d444. doi:10.1093/nar/gkab1061
21. Shityakov S, Förster C. In silico predictive model to determine vector-mediated transport properties for the blood-brain barrier choline transporter. *Adv Appl Bioinform Chem.* 2014;7:23–36. doi:10.2147/AABC.S63749
22. Rakhshani H, Dehghanian E, Rahati A. Enhanced GROMACS: toward a better numerical simulation framework. *J Mol Model.* 2019;25(12):355. doi:10.1007/s00894-019-4232-z
23. Van Der Spoel D, Lindahl E, Hess B, et al. GROMACS: fast, flexible, and free. *J Comput Chem.* 2005;26(16):1701–1718. doi:10.1002/jcc.20291
24. Valdés-Tresanco MS, Valdés-Tresanco ME, Valiente PA, et al. gmx_MMPBSA: A new tool to perform end-state free energy calculations with GROMACS. *J Chem Theory Comput.* 2021;17(10):6281–6291. doi:10.1021/acs.jctc.1c00645
25. Motrich RD, Maccioni M, Riera CM, et al. Autoimmune prostatitis: state of the art. *Scand J Immunol.* 2007;66(2–3):217–227. doi:10.1111/j.1365-3083.2007.01971.x
26. Yue SY, Niu D, Ma W-M, et al. The CXCL10/CXCR3 axis regulates Th1 cell differentiation and migration in experimental autoimmune prostatitis through the PI3K/AKT pathway. *Andrology.* 2023. doi:10.1111/andr.13571
27. Hua X, Zhang J, Chen J, et al. Sodium butyrate alleviates experimental autoimmune prostatitis by inhibiting oxidative stress and NLRP3 inflammasome activation via the Nrf2/HO-1 pathway. *Prostate.* 2024;84(7):666–681. doi:10.1002/pros.24683
28. Chaplan SR, Bach FW, Pogrel JW, et al. Quantitative assessment of tactile allodynia in the rat paw. *J Neurosci Meth.* 1994;53(1):55–63. doi:10.1016/0165-0270(94)90144-9

29. Dong Y, Wang X, Zhou Y, et al. Hypothalamus-pituitary-adrenal axis imbalance and inflammation contribute to sex differences in separation- and restraint-induced depression. *Horm Behav.* 2020;122:104741. doi:10.1016/j.yhbeh.2020.104741
30. Gulyás M, Bencsik N, Puzstai S, et al. AnimalTracker: An ImageJ-Based tracking API to create a customized behaviour analyser program. *Neuroinformatics.* 2016;14(4):479–481. doi:10.1007/s12021-016-9303-z
31. Zhang J, Yi Q-T, Gong M, et al. Upregulation of TRPV1 in spinal dorsal root ganglion by activating NGF-TrkA pathway contributes to pelvic organ cross-sensitisation in rats with experimental autoimmune prostatitis. *Andrologia.* 2019;51(8):e13302. doi:10.1111/and.13302
32. He H, Luo H, Qian B, et al. Autonomic nervous system dysfunction is related to chronic prostatitis/chronic pelvic pain syndrome. *World J Mens Health.* 2023;42:1–28. doi:10.5534/wjmh.220248
33. Roman K, Hall C, Schaeffer AJ, et al. TRPV1 in experimental autoimmune prostatitis. *Prostate.* 2020;80(1):28–37. doi:10.1002/pros.23913
34. Abbas MA. Modulation of TRPV1 channel function by natural products in the treatment of pain. *Chem Biol Interact.* 2020;330:109178. doi:10.1016/j.cbi.2020.109178
35. Yebe A, Toribio-Vazquez C, Martinez-Perez S, et al. Prostatitis: A review. *Curr Urol Rep.* 2023;24(5):241–251. doi:10.1007/s11934-023-01150-z
36. Song X, Chen G, Li C, et al. Tadalafil alleviates LPS-Induced inflammation and oxidative stress of RWPE-1 cell by regulating the Akt/Nrf2 signaling pathway. *Inflammation.* 2021;44(3):890–898. doi:10.1007/s10753-020-01384-w
37. Dos Santos Gomes FO, Oliveira AC, Ribeiro EL, et al. Intraurethral injection with LPS: an effective experimental model of prostatic inflammation. *Inflamm Res.* 2018;67(1):43–55. doi:10.1007/s00011-017-1094-7
38. Ye Y, Zhong W, Luo R, et al. Thermosensitive hydrogel with emodin-loaded triple-targeted nanoparticles for a rectal drug delivery system in the treatment of chronic non-bacterial prostatitis. *J Nanobiotech.* 2024;22(1):33. doi:10.1186/s12951-023-02282-7
39. Xu X, Hou J, Lv J, et al. Overexpression of lncRNA GAS5 suppresses prostatic epithelial cell proliferation by regulating COX-2 in chronic non-bacterial prostatitis. *Cell Cycle.* 2019;18(9):923–931. doi:10.1080/15384101.2019.1593644
40. Feng B, Dong Z, Wang Y, et al. Li-ESWT treatment reduces inflammation, oxidative stress, and pain via the PI3K/AKT/FOXO1 pathway in autoimmune prostatitis rat models. *Andrology.* 2021;9(5):1593–1602. doi:10.1111/andr.13027
41. Zhao X, Feng R, Chen J, et al. 4-Octyl itaconate alleviates experimental autoimmune prostatitis by inhibiting the NLRP3 inflammasome-induced pyroptosis through activating Nrf2/HO-1 pathway. *Prostate.* 2024;84(4):329–341. doi:10.1002/pros.24652
42. Sun D, Xing D, Wang D, et al. The protective effects of bushen daozhuo granule on chronic Non-bacterial prostatitis. *Front Pharmacol.* 2023;14:1281002. doi:10.3389/fphar.2023.1281002
43. Penna G, Amuchastegui S, Cossetti C, et al. Treatment of experimental autoimmune prostatitis in nonobese diabetic mice by the vitamin D receptor agonist eocalcitol. *J Immunol.* 2006;177(12):8504–8511. doi:10.4049/jimmunol.177.12.8504
44. Yongfeng Lao XG, Wang J, Bai Y, Zewen L, Wang Z, Dong Z. Molecular mechanism and promising treatments of chronic prostatitis/chronic pelvic pain syndrome: an exploratory bibliometric analysis and literature review of preclinical studies. *UroPrecision.* 2024;1(4):162–178.
45. Gao N, Li M, Wang W, et al. A bibliometrics analysis and visualization study of TRPV1 channel. *Front Pharmacol.* 2023;14:1076921. doi:10.3389/fphar.2023.1076921
46. Bujak JK, Kosmala D, Szopa IM, et al. Inflammation, cancer and immunity-implication of TRPV1 channel. *Front Oncol.* 2019;9:1087. doi:10.3389/fonc.2019.01087
47. Iftinca M, Defaye M, Altier C. TRPV1-targeted drugs in development for human pain conditions. *Drugs.* 2021;81(1):7–27. doi:10.1007/s40265-020-01429-2
48. Roman K, Murphy SF, Done JD, et al. Role of PAR2 in the development of lower urinary tract dysfunction. *J Urol.* 2016;196(2):588–598. doi:10.1016/j.juro.2016.01.106
49. Pattabiraman G, Engel G, Osborn CV, et al. Efficacy of targeted mast cell inhibition therapy in chronic prostatitis/chronic pelvic pain syndrome. *Urology.* 2023. doi:10.1016/j.urology.2023.05.047
50. Piao JJ, Kim S, Shin D, et al. Cannabidiol alleviates chronic prostatitis and chronic pelvic pain syndrome via CB2 receptor activation and TRPV1 desensitization. *World J Mens Health.* 2024. doi:10.5534/wjmh.230352
51. Yoshida A, Furube E, Mannari T, et al. TRPV1 is crucial for proinflammatory STAT3 signaling and thermoregulation-associated pathways in the brain during inflammation. *Sci Rep.* 2016;6:26088. doi:10.1038/srep26088
52. Yang XL, Wang X, Shao L, et al. TRPV1 mediates astrocyte activation and interleukin-1 β release induced by hypoxic ischemia (HI). *J Neuroinflamm.* 2019;16(1):114. doi:10.1186/s12974-019-1487-3
53. Chen L, Wang H, Ge S, et al. IL-6/STAT3 pathway is involved in the regulation of autophagy in chronic non-bacterial prostatitis cells, and may be affected by the NLRP3 inflammasome. *Ultrastruct Pathol.* 2021;45(4–5):297–306. doi:10.1080/01913123.2021.1966149